PCCP

COMMUNICATION

View Article Online
View Journal | View Issue

Cite this: *Phys. Chem. Chem. Phys.*, 2014, **16**, 672

Received 18th September 2013,
Accepted 4th November 2013

DOI: 10.1039/c3cp53946f

www.rsc.org/pccp

Controllable electronic energy structure of size-controlled Cu_2ZnSnS_4 nanoparticles prepared by a solution-based approach†

Hiroyasu Nishi,[a] Takahito Nagano,[a] Susumu Kuwabata[b] and Tsukasa Torimoto*[a]

Cu_2ZnSnS_4 nanoparticles with sizes of 2–5 nm, synthesized in hot organic solutions, exhibited size-dependent photoelectrochemical properties due to the quantum size effect. The potentials of the valence band edge and conduction band edge of the nanoparticles, experimentally determined by photoelectrochemical measurements, were shifted more positively and more negatively, respectively, with a decrease in particle size.

Compound semiconductors such as cadmium telluride (CdTe) and copper indium gallium selenide (CIGS) have been widely utilized as light-absorbing materials in solar cells because they have several advantages over conventional silicon-based solar cells: wide range absorption from the ultraviolet to visible wavelength region, tunable energy gap, high degree of stability, and high absorption coefficient.[1–3] Recently, a semiconductor of copper zinc tin sulfide (Cu_2ZnSnS_4) has attracted much attention in photovoltaic applications, because Cu_2ZnSnS_4 is composed of low-toxic and earth-abundant elements in addition to having an appropriate energy gap ($\sim$1.5 eV) for solar cell application.[4–7] So far, several research groups have reported on thin-film solar cells of Cu_2ZnSnS_4 or $Cu_2ZnSn(S,Se)_4$ showing energy conversion efficiencies of *ca.* 10%.[6,7] The efficiency has been greatly improved in recent years, and Cu_2ZnSnS_4 has become one of the promising materials for next-generation solar cells.

Cu_2ZnSnS_4 nanoparticles prepared by a solution-based strategy have also attracted great attention as precursors (nanocrystal ink) to fabricate a Cu_2ZnSnS_4 thin-film at a low cost.[8–12] For example, Korgel and co-workers have reported that Cu_2ZnSnS_4 nanoparticles prepared by thermal decomposition of metal precursors in a hot organic solution could be used as a light-absorbing layer in a photovoltaic device.[9] In our previous paper, we reported that Cu_2ZnSnS_4 nanoparticles with sizes of 5–6 nm exhibited photoelectrochemical properties which were similar to those of p-type semiconductor electrodes.[10] Agrawal and co-workers fabricated a $Cu_2ZnSn(S,Se)_4$ thin-film solar cell by sintering Cu_2ZnSnS_4 nanoparticles in Se vapor, exhibiting a solar energy conversion efficiency of 7.2%.[12] Moreover, size-quantized Cu_2ZnSnS_4 nanoparticles are regarded as an attractive candidate for a light-absorbing material in high-efficient quantum dot solar cells, whose theoretical conversion efficiency is expected to be higher than that predicted by the traditional Shockley–Queisser limit (32%).[13,14] Aydil and co-workers reported that the quantum size effect of Cu_2ZnSnS_4 nanoparticles became remarkable by decreasing the particle size to less than twice the exciton Bohr radius in a Cu_2ZnSnS_4 crystal.[15] Liu and co-workers reported the size dependence of the energy gap of Cu_2ZnSnS_4 nanoparticles prepared by a hydrothermal method.[16] In the case of efficient quantum dot-based solar cells, the determination of electronic energy structure, that is, the potentials of the valence band edge (E_{VB}) and conduction band edge (E_{CB}), is of considerable importance for size-quantized Cu_2ZnSnS_4 nanoparticles to estimate the energy band diagram formed in the devices. We previously reported that Cu_2ZnSnS_4 nanoparticles 5–6 nm in diameter had E_{VB} and E_{CB} values of +0.3 and −1.2 V *vs.* Ag/AgCl, respectively. However, there has been little investigation on the size dependence of energy levels.[10] In this study, we synthesized Cu_2ZnSnS_4 nanoparticles with average diameters ranging from 2.8 to 5.2 nm *via* a solution-based approach and we experimentally clarified the size dependence of the electronic energy structure.

Cu_2ZnSnS_4 nanoparticles were prepared by thermal decomposition of $Cu(S_2CNEt_2)_2$ (0.050 mmol), $Zn(S_2CNEt_2)_2$ (0.025 mmol),

[a] *Department of Crystalline Materials Science, Graduate School of Engineering, Nagoya University, Furo-cho, Chikusa-ku, Nagoya 464-8603, Japan. E-mail: torimoto@apchem.nagoya-u.jp; Fax: +81-52-789-5299; Tel: +81-52-789-4614*

[b] *Department of Applied Chemistry, Graduate School of Engineering, Osaka University, 2-1 Yamadaoka, Suita, Osaka 565-0871, Japan*

† Electronic supplementary information (ESI) available: Reaction conditions, particle size, and chemical compositon of the Cu_2ZnSnS_4 nanoparticles are summarized in Table S1. XRD diffraction patterns and Raman scattering spectrum of the Cu_2ZnSnS_4 nanoparticles are shown in Fig. S1 and S2, respectively. Fig. S3 displays Tauc plots to determine E_g. A typical change in absorption spectra along with the layer-by-layer deposition process is shown in Fig. S4. PES spectra of the Cu_2ZnSnS_4 nanoparticles are shown in Fig. S5. See DOI: 10.1039/c3cp53946f

and $Sn(S_2CNEt_2)_4$ (0.025 mmol) in 1-dodecanethiol (DDT) with addition of a small amount of oleylamine (OLA) (0.13–2.0 mmol) at 120–280 °C for 30 min under an N_2 atmosphere. The metal complex of $Sn(S_2CNEt_2)_4$ was prepared by a method described in ref. 15. The total volume of DDT and OLA was set to 3.0 cm^3. OLA was added in order to promote the decomposition of diethyldithiocarbamates, which acted as metal and sulfur sources.[17] To control the particle size, the amount of OLA added and/or the reaction temperature were systematically varied (Table S1, ESI†), with the average diameter of Cu_2ZnSnS_4 nanoparticles being enlarged with an increase in the amount of OLA added or with elevation of the reaction temperature. After cooling to ambient temperature, the resulting solution was centrifuged at 4000 rpm to remove large precipitates. Ethanol was added to the supernatant and the mixture was centrifuged at 4000 rpm. Finally, Cu_2ZnSnS_4 nanoparticles, obtained as precipitates, were washed with ethanol.

Fig. 1a and b show typical TEM images of Cu_2ZnSnS_4 nanoparticles prepared by the addition of 0.13 and 2.0 mmol of OLA, respectively, at 150 °C. Nanometer-sized spherical particles were formed in each condition, and the average diameters of the particles (d) shown in Fig. 1a and b were determined to be 2.8 ± 0.4 and 3.5 ± 0.7 nm, respectively, from the TEM images (Table S1, ESI†), indicating that the size of the particles increased with an increase in the amount of OLA added. Fig. 1c and d show particles prepared at 120 and 280 °C, respectively, with the addition of 0.50 mmol of OLA. Spherical or polygonal nanoparticles with d of 2.9 ± 0.5 and 5.2 ± 0.9 nm were formed by reactions at 120 and 280 °C, respectively. Energy dispersive X-ray (EDX) analyses revealed that the atomic ratios of Cu : Zn : Sn in the particles shown in Fig. 1a–d were 0.47 : 0.25 : 0.28, 0.44 : 0.24 : 0.32, 0.46 : 0.23 : 0.31, and 0.47 : 0.21 : 0.32, respectively. The content of S^{2-} in the Cu_2ZnSnS_4 nanoparticles prepared in this study could not be precisely determined due to the presence of the surface adsorbed DDT molecules having a –SH group. These indicated that Cu-poor and Sn-rich particles were formed, the composition being roughly constant regardless of the particle size. Furthermore, broad peaks assigned to kesterite-type Cu_2ZnSnS_4 were observed in the XRD diffraction pattern without any peaks being assigned to secondary phases such as Cu_2S or SnS_2 (Fig. S1, ESI†). The average sizes of the nanoparticles estimated from full width at half maximum of XRD diffraction peaks using the Scherrer equation were approximately in accordance with the diameters determined from corresponding TEM images (Table S1, ESI†), suggesting that most of the obtained particles were single-crystal nanoparticles. The formation of a Cu_2ZnSnS_4 crystal phase was also confirmed by Raman spectra, in which only a signal of 338 cm^{-1}, assigned to A_1 symmetry of kesterite Cu_2ZnSnS_4, was observed (Fig. S2, ESI†).[18,19] Consequently, we successfully controlled the diameter of the Cu_2ZnSnS_4 nanoparticles from 2.8 to 5.2 nm without changing the chemical composition and crystalline structure.

In order to evaluate the size dependence of the electronic energy structure, the energy gap (E_g) of Cu_2ZnSnS_4 nanoparticles was estimated from the absorption spectra shown in Fig. 2a. The absorption spectra varied greatly depending on the size of Cu_2ZnSnS_4 nanoparticles, and the onset wavelength was

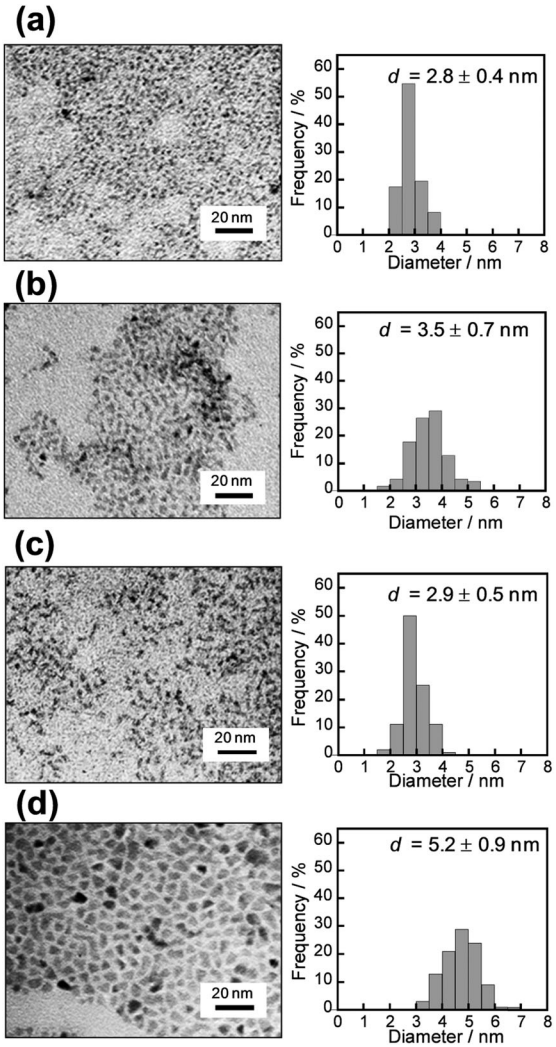

Fig. 1 TEM images of Cu_2ZnSnS_4 nanoparticles prepared by addition of (a) 0.13 mmol of OLA at 150 °C, (b) 2.0 mmol of OLA at 150 °C, (c) 0.50 mmol of OLA at 120 °C, and (d) 0.50 mmol of OLA at 280 °C. The size distributions of the nanoparticles are shown next to the corresponding TEM images.

shifted to a higher energy with a decrease in particle size due to the quantum size effect. Fig. 2b shows the relationship between d of Cu_2ZnSnS_4 nanoparticles and their E_g determined from Tauc plots of the results shown in Fig. 2a (Fig. S3, ESI†). The relationship between the diameter and the E_g of the particles reported in ref. 15 and 16 is also shown in the figure. The size dependence of the E_g of Cu_2ZnSnS_4 nanoparticles prepared in the present study corresponded well to previously reported ones. Cu_2ZnSnS_4 particles with diameters larger than *ca.* 5 nm had an E_g similar to that of the bulk value, $E_{g\,bulk}$ = 1.45 eV,[20] while the E_g of particles with diameters smaller than *ca.* 5 nm increased rapidly with a decrease in particle size. This behavior is in agreement with that theoretically expected: the quantum size effect observed for particles with diameters smaller than twice the Bohr radius (a_B = 2.5–3.3 nm for Cu_2ZnSnS_4 crystal) was remarkable.[15] As mentioned in the previous section, the chemical composition of the resulting particles was almost

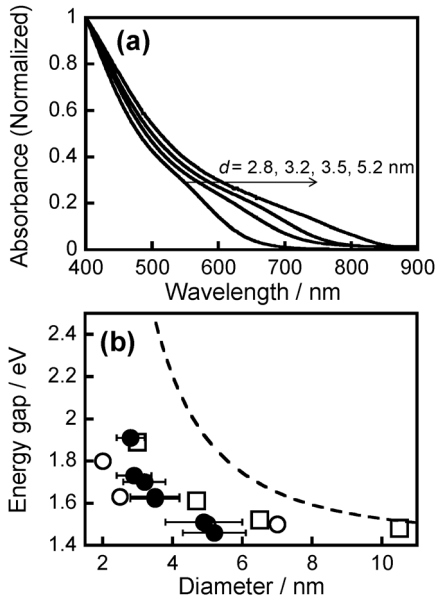

Fig. 2 (a) Absorption spectra of Cu_2ZnSnS_4 nanoparticles with various diameters. (b) Plots of E_g as a function of d of Cu_2ZnSnS_4 nanoparticles (solid circles). Open circles and open squares represent data reported in ref. 15 and 16, respectively. Error bars represent standard deviation of the diameters. The broken line represents theoretical values calculated using the infinite-depth-well model.

constant regardless of the particle size. Therefore, the change in the E_g value shown in Fig. 2b originated from the quantum size effect as in the case of particles reported in ref. 15 and 16, not from change in the chemical composition of Cu_2ZnSnS_4 nanoparticles.

The infinite-depth-well model enables preliminary estimation of the size-dependent E_g of semiconductor nanoparticles.[21–23] As shown in Fig. 2b, the theoretical relationship between d and E_g of Cu_2ZnSnS_4 nanoparticles was calculated by using the electron and hole effective masses ($m_e^* = 0.18\ m_0$ and $m_h^* = 0.22\ m_0$, respectively),[24] $E_{g\,bulk}$ (1.45 eV),[20] and relative dielectric constant ($\varepsilon_r = 6.7$)[24] for a Cu_2ZnSnS_4 crystal. It was found that the infinite-depth-well model could roughly reproduce the tendency in the experimental data, that is, the enlargement of E_g with a decrease in d, but the calculated value at each particle size was considerably overestimated in comparison with the experimentally obtained E_g, which is similar to the cases reported for other multinary semiconductor nanoparticles such as $CuInS_2$ and $AgInS_2$ nanoparticles.[25,26]

To determine E_{VB} and E_{CB} for the Cu_2ZnSnS_4 nanoparticles, photoelectrochemical measurements were carried out using nanoparticles immobilized on an ITO-coated glass electrode. The particles were immobilized by alternatively dipping a cleaned ITO electrode into an ethanol solution of 1,2-ethanedithiol (0.10 mol dm^{-3}) and a hexane solution of Cu_2ZnSnS_4 nanoparticles with an absorbance of 0.30 at 500 nm in a quartz cuvette with 1 mm optical path length. This layer-by-layer deposition process was repeated for ~10 cycles (Fig. S4, ESI†). The photoelectrochemical properties of the thus-obtained nanoparticulate film electrodes were measured in an $Eu(NO_3)_3$ aqueous solution (0.2 mol dm^{-3}). The potential was determined against an Ag/AgCl (sat. KCl) reference electrode and a Pt wire was used as a counter electrode.

Fig. 3a and b show photocurrent–potential (I–V) curves of the thus-obtained Cu_2ZnSnS_4 nanoparticle electrodes with d of 2.8 ± 0.4 and 4.9 ± 1.1 nm, respectively. A cathodic photocurrent was observed under light irradiation (λ > 350 nm) in each electrode, indicating that the immobilized nanoparticles behaved as a p-type semiconductor regardless of the particle size. The action spectra of the cathodic photocurrent agreed well with the absorption spectra of the corresponding nanoparticles as shown in the insets of Fig. 3a and b. Thus, it can be concluded that the cathodic photocurrent was produced by photoexcitation of Cu_2ZnSnS_4 particles on the ITO electrodes.

In bulk p-type semiconductor electrodes, photogenerated holes diffuse inside the semiconductor and then can be injected into a contacting electrode as long as the electrode potential is more negative than that of the flatband potential (E_{FB}). It is reasonably assumed in many instances of p-type semiconductors that E_{FB} is comparable to the potential of E_{VB}. Thus, the onset potentials of the cathodic photocurrent shown in Fig. 3a and b, corresponding to E_{FB}, could be regarded as E_{VB} and were determined to be +0.38 and +0.20 V *vs.* Ag/AgCl for the Cu_2ZnSnS_4 nanoparticles with d of 2.8 ± 0.4 and 4.9 ± 1.1 nm,

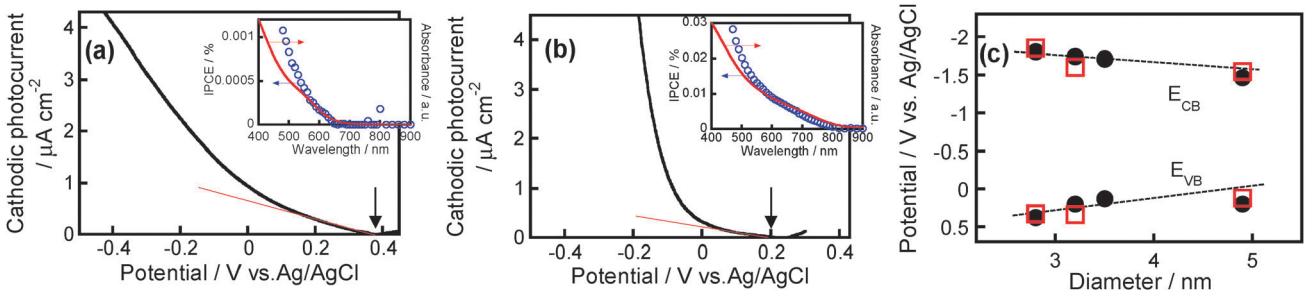

Fig. 3 Photocurrent–potential curves of Cu_2ZnSnS_4 nanoparticles with d of (a) 2.8 ± 0.4 nm and (b) 4.9 ± 1.1 nm immobilized on ITO electrodes. The photocurrent was detected using a potentiostat and amplified using a lock-in amplifier. The insets show action spectra of the cathodic photocurrent under an applied potential of −0.5 V *vs.* Ag/AgCl. The solid lines in the insets represent the absorption spectra of corresponding Cu_2ZnSnS_4 nanoparticles. (c) Relationships between d and potentials of E_{VB} and E_{CB} of Cu_2ZnSnS_4 nanoparticles determined by photoelectrochemical measurements (solid circles) and PES (open squares).

respectively, by extrapolating the linear part of the current–potential curve near the photocurrent onset. Furthermore, E_{CB} can be calculated by the following equation:[26,27]

$$E_g = E_{VB} - E_{CB} + E_{Coulomb}, \quad (1)$$

where E_g is the energy gap of Cu_2ZnSnS_4 nanoparticles determined from absorption spectra, $E_{Coulomb}$ is the Coulomb interaction energy between an electron and a hole given by $-1.8e^2/(2\pi\varepsilon_r\varepsilon_0 d)$, and e and ε_0 represent the electronic charge and the permittivity of free space, respectively. Fig. 3c shows the potentials of E_{VB} and E_{CB} of Cu_2ZnSnS_4 nanoparticles as a function of average diameter. E_{VB} and E_{CB} were shifted to positive and negative potentials, respectively, with a decrease in d, as expected from the quantum size effect. This indicated that the quantum confinement of the charge carriers in the semiconductor nanoparticles changed their electronic energy structure, the degree being remarkable with a decrease in particle size. Fig. 3c also shows the electronic energy structure determined by photo-electron spectroscopy (PES) using a Riken Keiki AC-2 photoelectron spectrometer. PES could determine the ionization energy corresponding to the potential of E_{VB} in a semiconductor as compared to the vacuum level,[28] −4.64 V *vs.* Ag/AgCl (Fig. S5, ESI†), while E_{CB} was obtained using eqn (1) as well as by the photoelectrochemical measurements. The potentials of E_{VB} and E_{CB} of PES corresponded well to those determined from photoelectrochemical measurements, indicating the accuracy of the potentials of E_{VB} and E_{CB} determined in the present study.

In conclusion, we successfully controlled the diameter of Cu_2ZnSnS_4 nanoparticles in the range of 2.8–5.2 nm by changing the reaction conditions without varying the chemical composition and crystal structure. The potential of E_{VB} shifted positively from +0.20 to +0.38 V *vs.* Ag/AgCl and E_{CB} shifted negatively from −1.47 to −1.81 V *vs.* Ag/AgCl with a decrease in d from 4.9 to 2.8 nm. The presence of a size-dependent electronic energy structure will require precise size control of Cu_2ZnSnS_4 nanoparticles for their application in photovoltaic devices. The findings in the present study will therefore be important for investigating and designing the energy band diagram in quantum dot-based solar cells fabricated using Cu_2ZnSnS_4 nanoparticles.

Acknowledgements

This work was supported by a Funding Program for Next Generation World-Leading Researchers (NEXT Program) from the Japan Society for the Promotion of Science.

Notes and references

1 G. Khrypunov, A. Remeo, F. Kurdeasu, D. L. Bätzner, H. Zogg and A. N. Tiwari, *Sol. Engery Mater. Sol. Cells*, 2006, **90**, 664.
2 P. Jackson, D. Hariskos, E. Lotter, S. Paetel, R. Wuerz, R. Menner, W. Wischmann and M. Powalla, *Prog. Photovoltaics: Res. Appl.*, 2011, **19**, 894.
3 I. Repins, M. A. Contreras, B. Egaas, C. DeHart, J. Scharf, C. L. Perkins, B. To and R. Noufi, *Prog. Photovoltaics: Res. Appl.*, 2008, **16**, 235.
4 K. Ramasamy, M. A. Malik and P. O'Brien, *Chem. Commun.*, 2012, **48**, 5703.
5 S. Delbos, *EPJ Photovoltaics*, 2012, **3**, 35004.
6 T. K. Todorov, J. Tang, S. Bag, O. Gunawan, T. Gokmen, Y. Zhu and D. B. Mitzi, *Adv. Energy Mater.*, 2013, **3**, 34.
7 D. A. R. Barkhouse, O. Gunawan, T. Gokmen, T. K. Todorov and D. B. Mitzi, *Prog. Photovoltaics: Res. Appl.*, 2012, **20**, 6.
8 S. C. Riha, B. A. Parkinson and A. L. Prieto, *J. Am. Chem. Soc.*, 2009, **131**, 12054.
9 C. Steinhagen, M. G. Panthani, V. Akhavan, B. Goodfellow, B. Koo and B. A. Korgel, *J. Am. Chem. Soc.*, 2009, **131**, 12554.
10 T. Kameyama, T. Osaki, K. Okazaki, T. Shibayama, A. Kudo, S. Kuwabata and T. Torimoto, *J. Mater. Chem.*, 2010, **20**, 5319.
11 Q. Guo, H. W. Hillhouse and R. Agrawal, *J. Am. Chem. Soc.*, 2009, **131**, 11672.
12 Q. Guo, G. M. Ford, W.-C. Yang, B. C. Walker, E. A. Stach, H. W. Hillhouse and R. Agrawal, *J. Am. Chem. Soc.*, 2010, **132**, 17384.
13 W. Shockley and H. J. Queisser, *J. Appl. Phys.*, 1961, **32**, 510.
14 A. J. Nozik, M. C. Beard, J. M. Luther, M. Law, R. J. Ellingson and C. Johnson, *Chem. Rev.*, 2010, **110**, 6873.
15 A. Khare, A. W. Wills, L. M. Ammerman, D. J. Norris and E. S. Aydil, *Chem. Commun.*, 2011, **47**, 11721.
16 W. C. Liu, B. L. Guo, X. S. Wu, F. M. Zhang, C. L. Mak and K. H. Wong, *J. Mater. Chem. A*, 2013, **1**, 3182.
17 Y. K. Jung, J. I. Kim and J.-K. Lee, *J. Am. Chem. Soc.*, 2010, **132**, 178.
18 M. Himmrich and H. Haeuseler, *Spectrochim. Acta*, 1991, **47A**, 933.
19 P. A. Fernandes, P. M. P. Salomé and A. F. da Cunha, *J. Alloys Compd.*, 2011, **509**, 7600.
20 K. Ito and T. Nakazawa, *Jpn. J. Appl. Phys.*, 1988, **27**, 2094.
21 Y. Kayanuma, *Phys. Rev. B: Condens. Matter Mater. Phys.*, 1988, **38**, 9797.
22 S. Barik, A. K. Srivastava, P. Misra, R. V. Nandedkar and L. M. Kukreja, *Solid State Commun.*, 2003, **127**, 463.
23 L. E. Brus, *J. Chem. Phys.*, 1984, **80**, 4403.
24 C. Persson, *J. Appl. Phys.*, 2010, **107**, 053710.
25 T. Omata, K. Nose and S. Otsuka-Yao-Matsuo, *J. Appl. Phys.*, 2009, **105**, 073106.
26 T. Torimoto, M. Tada, M. Dai, T. Kameyama, S. Suzuki and S. Kuwabata, *J. Phys. Chem. C*, 2012, **116**, 21895.
27 Y. Nosaka, *J. Phys. Chem.*, 1991, **95**, 5054.
28 J. Jasieniak, M. Califano and S. E. Watkins, *ACS Nano*, 2011, **7**, 5888.